ACS APPLIED ENERGY MATERIALS

www.acsaem.org Article

High-Quality $SnSe_2$ Single Crystals: Electronic and Thermoelectric Properties

Anh-Tuan Pham, Thi Hoa Vu, Chang Cheng, Thi Ly Trinh, Ji-Eun Lee, Hyejin Ryu, Choongyu Hwang, Sung-Kwan Mo, Jungdae Kim, Li-dong Zhao, Anh-Tuan Duong,* and Sunglae Cho*

Cite This: https://dx.doi.org/10.1021/acsaem.0c01846 Read Online

ACCESS | Metrics & More | Article Recommendations

ABSTRACT: High-quality $SnSe_2$ single crystals were successfully synthesized using a temperature gradient method. N-type characteristics and strong anisotropic transport properties of $SnSe_2$ single crystals were exhibited between the ab plane and the *c*-axis. At 673 K, the power factor (PF) value along the ab plane is 3.43 μW cm^{-1} K^{-2}, while it is 0.92 μW cm^{-1} K^{-2} along the *c*-axis. The ratio between thermal conductivities along the ab plane (κ_{ab}) and *c*-axis (κ_c) is on the order of 7.6 at 300 K, while this value is about 5.6 at 673 K. The thermoelectric figure of merit (ZT) in the *c*-axis (0.15) is higher than that (0.1) along the ab plane, according to the ultralow out-of-plane thermal conductivity. The electronic band structure results, which were examined by angle-resolved photoemission spectroscopy (ARPES) predicted the potential of improving the thermoelectric performance of $SnSe_2$ single crystals by electron doping.

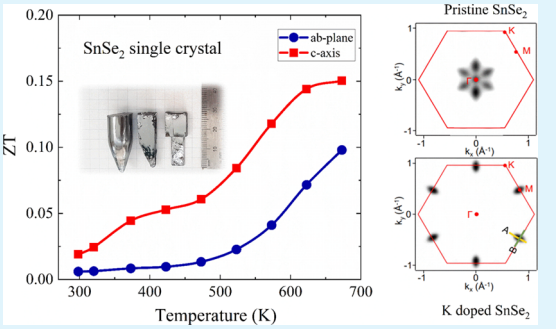

KEYWORDS: *thermoelectric material, single crystal, $SnSe_2$, ultralow thermal conductivity, ARPES*

1. INTRODUCTION

Recently, thermoelectric materials, which directly convert waste heat into electricity, have attracted increasing attention. The thermoelectric performance is evaluated by the dimensionless thermoelectric figure of merit, $ZT = \frac{S^2\sigma T}{\kappa}$, where S, σ, T, and κ represent the Seebeck coefficient, electrical conductivity, absolute temperature, and thermal conductivity, respectively.[1,2] To reach excellent performance as a commercial product, S and σ should stay at high values, while κ should remain low. Since these three transport coefficients are interdependent, it is difficult to optimize the ZT value. There are typical ways to improve the ZT value such as enhancing the power factor (PF, $S^2\sigma$) via optimizing the carrier concentration (n) and mobility (μ) or suppressing the lattice thermal conductivity (κ_L) by introducing the scattering centers. As a result, there are currently only a few materials used for commercial applications.

In layered structure materials, the difference in the bonding mechanism between in-plane and out-of-plane leads to unique electronic and thermal transport properties. Among them, layered chalcogenide crystals possessing strong intralayer covalent bonding and noticeable weak interlayer van der Waals bonding, such as Bi_2Te_3 and Sb_2Te_3, are by far recognized as good thermoelectric materials at around room temperature. In addition, layered SnSe with weak cross-plane covalent bonds, has been reported with in-plane ZT = 2.6 at 923 K in p-type SnSe,[3] ZT = 2.2 at 733 K in Bi-doped n-type SnSe,[4] and out-of-plane ZT = 2.8 at 773 K in Br-doped n-type SnSe.[5]

In the family of layered structure materials, tin diselenide ($SnSe_2$) possesses a CdI_2-type hexagonal structure with space group $P\bar{3}m1$, which is formed by van der Waals bonding between Sn−Se−Sn slabs along the out-of-plane direction (*c*-axis). Lattice parameters of $SnSe_2$ are a = 3.811 Å and c = 6.137 Å.[6] $SnSe_2$ has yet been confirmed to belong to n-type semiconductors with an indirect band gap of 0.97 eV,[7] which was considered in applications such as phase-change memory, optoelectronic devices, field-effect transistors (FETs), and gas sensor devices.[8−12] Recently, $SnSe_2$ has attracted interest from scientists due to its ultralow thermal conductivity. Some theoretical calculations have predicted that thermoelectric properties of $SnSe_2$ are significantly influenced by the carrier concentration. A ZT value for a p-type $SnSe_2$ monolayer of up to 0.94 at 600 K can be obtained with a carrier concentration of around 10^{19} cm^{-3}, while it is around 0.8 for n-type $SnSe_2$ with a carrier concentration of around 10^{20} cm^{-3}.[13] Ding et al.

Received: August 1, 2020
Accepted: September 25, 2020
Published: September 25, 2020

predicted that the ZT values of n-type $SnSe_2$ are 0.01, 0.2, 1.1, and 2.95 at 800 K with carrier concentrations of 10^{17}, 10^{18}, 10^{19}, and 10^{20} cm^{-3}, respectively.[14] By doping Cl, Xu et al. achieved ZT = 0.4 at 673 K in $SnSe_{1.88}Cl_{0.12}$ polycrystals.[15] By doping Ag, Li et al. also obtained ZT = 0.4 in $Sn_{0.99}Ag_{0.01}Se_2$ at 773 K.[16] By substituting Br into Se sites of $SnSe_2$, Wu et al. improved the ZT to 0.6 at 750 K.[17]

Based on the potential applications of $SnSe_2$ crystals, the synthesis of high-quality $SnSe_2$ single crystals is beneficial to study the intrinsic thermoelectric properties. In this article, high crystalline quality $SnSe_2$ has been grown by a simple temperature gradient method and its anisotropic thermoelectric transport properties have been studied. The thermoelectric performance of $SnSe_2$ single crystals is better than that of polycrystalline. Besides, the angle-resolved photoemission spectroscopy (ARPES) results show the potential for improving thermoelectric performance by electron doping.

2. EXPERIMENTAL SECTION

$SnSe_2$ single crystals were grown by the temperature gradient method.[18] First, high-purity (5N) Se and Sn powders in a mole ratio of 2:1 were weighed and sealed in a quartz ampoule under vacuum (<10^{-4} Torr). Then, the ampoule was heated to 750 °C (60 °C h^{-1}) and soaked for 10 h. Finally, the temperature was gradually decreased with a rate of 1 °C h^{-1} to 550 °C and then rapidly decreased to room temperature (50 °C h^{-1}). High-quality $SnSe_2$ crystals with sizes of 14 mm diameter × 30 mm length were obtained. The crystal structure was studied by means of X-ray diffraction (XRD). Field-emission scanning electron microscopy (FE-SEM) and energy-dispersive X-ray spectroscopy (EDS) were used to observe the layer morphology and stoichiometry of the samples, respectively.

To study the thermoelectric properties in both directions, parallel (ab plane) and perpendicular (*c*-axis) to the layered plane, bar-shaped samples used to measure the Seebeck coefficient and electrical conductivity and disk-shaped samples used to measure the thermal diffusivity were cut into precise sizes of 3 × 3 x 10 mm^3 and 13 × 13 × 1 mm^3, respectively. The Seebeck coefficient and electrical conductivity were determined simultaneously in an Argon environment to prevent oxidation and evaporation. Hall measurements were performed at various temperatures from 300 to 673 K via the van der Pauw method under a reversible magnetic field of 0.7 T. The laser flash diffusivity method (LFA-457, NETZSCH, Germany) was used to evaluate the thermal diffusivity (D). The heat capacity was determined from the measured values of Wiedemeier et al.[19] by C_p = 73.39 + 1.15 × $10^{-2}T$ − 1.92 × 10^5T^{-2} (J K^{-1} mol^{-1}) with an uncertainty of 1% for $SnSe_2$. The total thermal conductivity was obtained following the formula $\kappa_{tot} = D \cdot C_p \cdot \rho$, where ρ is the mass density measured by the Archimedes principle at 300 K. The lattice thermal conductivity (κ_L) was obtained by subtracting the electronic contribution ($\kappa_e = LT/\rho$) from the total thermal conductivity (κ_{tot}), where the Lorenz number[20] ($L \sim \left[1.5 + \exp\left(-\frac{|S|}{116}\right)\right] \times 10^{-8}$ W Ω K^{-2}) was estimated from the Seebeck coefficient data. Transport property measurements (S, σ, and κ) were conducted from room temperature to 673 K, with an uncertainty of ~5% for each parameter. Angle-resolved photoemission spectroscopy (ARPES) was performed at Beamline 10.0.1, Advanced Light Source, using a photon energy of 55 eV. The measurements were performed under a base pressure below 4 × 10^{-11} Torr at 30 K.

3. RESULTS AND DISCUSSION

Using the temperature gradient method, we have been successfully grown high-quality $SnSe_2$ single crystals. Figure 1a describes the real image of the grown samples with cleaved shiny surfaces. EDS measurements indicate that the ratio of Se to Sn is 2:1, as shown in Figure 1b. The surface of a cleaved $SnSe_2$ single crystal was observed by FE-SEM. The results

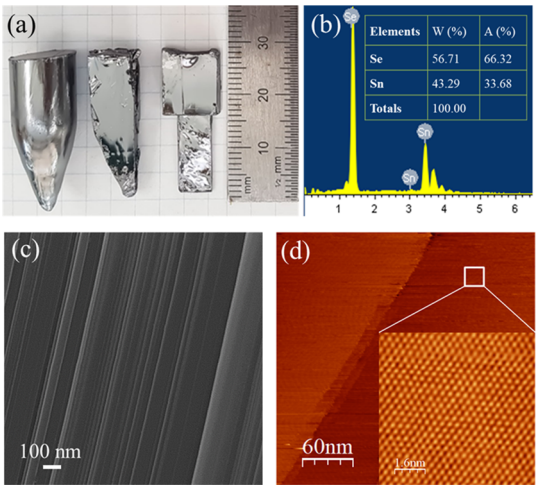

Figure 1. (a) Photo of samples, (b) EDS measurement data, (c) FE-SEM image, and (d) STM image of the $SnSe_2$ single crystal.

exhibited a clear surface and a lamellar microstructure with an average thickness of a few tens of nanometers, as shown in Figure 1c. For STM (scanning tunneling microscopy) studies, the sample was cleaved in situ to obtain clean surfaces of $SnSe_2$ single crystals. The high-resolution STM image in Figure 1d proved the appearance of a hexagonal structure of Se on the surface of $SnSe_2$.

The XRD result of cleaved $SnSe_2$ single crystals without any impure peaks is shown in Figure 2a. Compared with JCPDS

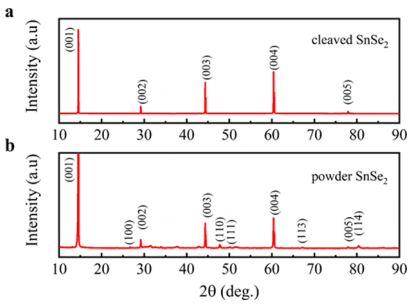

Figure 2. Room-temperature XRD patterns of (a) cleaved and (b) powdered $SnSe_2$.

PDF 89-3197 data, all diffraction peaks belong to the hexagonal $SnSe_2$ structure and the patterns showed only (00l) peak group. Lattice parameters of $SnSe_2$ single crystals were calculated from powder XRD data (as shown in Figure 2b) with Cu Kα_1 radiation; a = 3.808 Å and c = 6.129 Å are comparable to those reported earlier. The calculated mass density of the grown $SnSe_2$ single crystal by lattice parameters is 5.966 g cm^{-3}, which agreed well with that of the directly measured one, 5.937 ± 0.11 g cm^{-3}.

Figure 3a represents the temperature dependence of carrier concentration ($n(T)$), which is obtained from Hall measurements by the formula $\frac{V_H}{I} = \frac{1}{ned}H$, where V_H is the Hall voltage, I is the current, n is the number of carriers, e is the electrical charge, H is the magnetic field, and d is the sample thickness. With increasing temperature, n gradually increases from 2.26 × 10^{-18} cm^{-3} at 300 K to 3.37 × 10^{18} cm^{-3} at 473 K and then dramatically increases up to 3.05 × 10^{19} cm^{-3} at 673 K. The number of carriers at 300 K is one order of magnitude higher

https://dx.doi.org/10.1021/acsaem.0c01846
ACS Appl. Energy Mater. XXXX, XXX, XXX−XXX

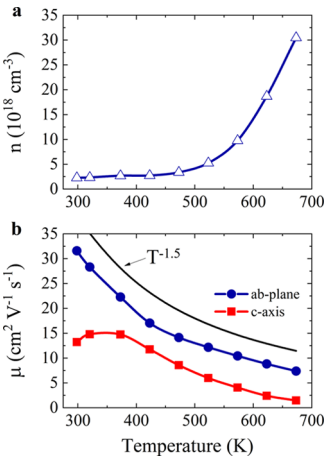

Figure 3. Temperature dependence of (a) carrier concentrations and (b) carrier mobility of $SnSe_2$ single crystals.

than that for the previously reported single crystal by Julien *et al.* prepared by the Bridgman technique, while the electron mobility along the ab plane, μ = 31.6 cm^2 V^{-1} s^{-1} (Figure 3b), is quite similar.[6] The mobility along both directions decreases sharply with temperature and obeys the trend of $T^{-3/2}$, pointing out that the acoustic phonon scattering is the major contribution. These results are reasonable compared with those of previous works on single crystals and polycrystals of $SnSe_2$. However, the mobility value in the single crystal is much higher than those in polycrystalline samples.[6,21−23] Thermoelectric properties of $SnSe_2$ single crystals have been measured along the cleaved surface (ab plane) and perpendicular cleaved surface (*c*-axis) from 300 to 673 K, as shown in Figure 4. Electrical conductivity showed semiconducting behavior. However, measurement results along the cleaved surface and perpendicular cleaved surface are different due to the anisotropic transport properties of this material. Especially at above 500 K, the electrical conductivity along the cleaved plane (σ_{ab}) increases up to 35.97 S cm^{-1} at 673 K

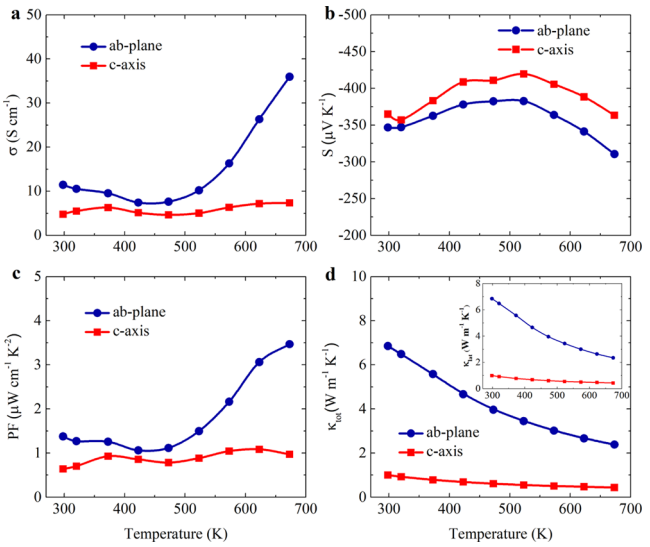

Figure 4. Temperature-dependent thermoelectric transport properties along both directions. (a) Electrical resistivity ($\sigma(T)$), (b) Seebeck coefficient ($S(T)$), (c) power factor ($S^2\sigma$), and (d) thermal conductivity ($\kappa(T)$).

because of the rapid increase of carrier concentration. The Seebeck coefficient along and perpendicular to the cleaved surface follows a similar trend, as shown in Figure 4b. From room temperature to 500 K, $SnSe_2$ single crystals exhibited the metallic transport behavior. This transport behavior can also be observed in Figure 3b when the carrier mobility exhibits a sharp degradation and, in contrast, the carrier concentration increases slightly along with the temperature. As generally expected, Seebeck coefficients slowly increase with the temperature, which corresponds to the decrease of electrical conductivity. At above 500 K, the sample shows thermally activated transport behavior. So, both the electrical conductivity and Seebeck coefficient show an opposite trend compared to those at lower temperatures. Figure 4c shows the thermoelectric power factor (PF = S^2 σ) along both directions. The maximum *PF* along the cleaved plane (3.47 μW cm^{-1} K^{-2}) is larger than that along the *c*-axis direction (0.97 μW cm^{-1} K^{-2}) owing to the relatively large difference in electrical conductivities between the two directions. Furthermore, its anisotropy becomes stronger with temperature. Because of the limitation of material thermal stability, it is impractical to carry out the experiment at higher temperatures. Therefore, peak electrical conductivities are not obtained in this temperature range, and the highest value is around 35.97 S cm^{-1} at 673 K.

Temperature-dependent total thermal conductivities (κ_{tot}) along and perpendicular to the cleaved surface are shown in Figure 4d. The data revealed that the lattice thermal conductivity accounts for 98% of κ_{tot}; phonon transport contributed to most total heat transfer in $SnSe_2$. From the inset, the lattice thermal conductivities (in-plane and out-of-plane) decrease as T^{-1} along with temperature; this could result from the anharmonic phonon−phonon interactions. In addition, the obtained in-plane thermal conductivity (κ_{ab}) is significantly larger than the out-of-plane one (κ_c) at all temperatures. At 300 K, we found κ_{ab} = 6.9 W m^{-1} K^{-1}, which is nearly eight times higher than κ_c = 0.9 W m^{-1} K^{-1}. The ratio κ_{ab}/κ_c = 7.6 indicates strong anisotropy in the thermal conductivity of $SnSe_2$. Moreover, at 673 K, the out-of-plane κ_c even drops to an ultralow value of 0.43 W m^{-1} K^{-1}. The large anisotropy in thermal transport properties is well explained by the crystal structure and bonding characters of $SnSe_2$. This is a consequence of ultraweak van der Waals forces among layers compared with the intralayer covalent bonding. These values agree well with both previous experimental[24] and theoretical studies.[14,25]

The ZT values along and perpendicular to the cleaved surface are shown in Figure 5. The ZT values of both directions increase with temperature. Ultralow out-of-plane

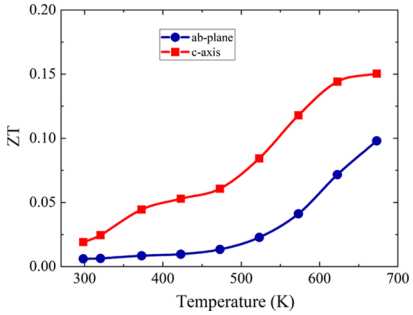

Figure 5. Temperature-dependent dimensionless figure of merit (ZT) of $SnSe_2$ along both directions.

https://dx.doi.org/10.1021/acsaem.0c01846
ACS Appl. Energy Mater. XXXX, XXX, XXX−XXX

thermal conductivity is the cause of higher ZT_c value compared to the ab-plane ZT_{ab}. We determine that the maximum ZT value of $SnSe_2$ single crystals along the *c*-axis direction is 0.15 at 673 K, while that along the ab plane is 0.1. Note that, in previous experiment reports, the ZT value of the undoped $SnSe_2$ polycrystal is usually smaller, 0.05.[9,10] In two theoretical calculations by Li et al. and Ding et al., the ZT values of the monolayer and single crystal of $SnSe_2$ are strongly dependent on the carrier concentration. For the n-type $SnSe_2$ monolayer, the ZT value at 900 K with an electron concentration of 10^{18} cm^{-3} is 0.1 and increases up to 1.1 with *n* of 10^{20} cm^{-3}. For the $SnSe_2$ single crystal, the ZT value at 800 K is 0.15 with $n \approx 10^{18}$ cm^{-3} and increases up to 2.95 with $n \approx 10^{20}$ cm^{-3}.[14,26]

To study the relation between ZT and electronic band structure, we analyze the electronic band structure of $SnSe_2$ single crystals using ARPES. The overall band structure obtained from ARPES experiments is consistent with the reported theoretical results.[27,28] The position of the valence band maximum (VBM) of pristine $SnSe_2$ is 1.36 eV below Fermi energy (E_F) with no photoemission intensity near E_F, implying that $SnSe_2$ is an intrinsic *n*-type semiconductor (Figure 6a,b). The constant energy contour at VBM shows a flowerlike shape, indicating the three-fold rotational symmetry of $SnSe_2$. By potassium (K) doping, $SnSe_2$ is electron-doped so that the conduction bands are clearly revealed at the M point (Figure 6c), which is comparable to the earlier calculation result.[27] The extracted effective masses from the conduction band of $SnSe_2$ are $m_{\Gamma-M}^* = (2.63 \pm 0.12)m_e$ and $m^*_{K-M} = (1.56 \pm 0.10)m_e$ (Figure 6d), which are similar to the theoretical value.[29] Note that the ARPES measurement is performed at 30 K to illustrate the band structure clearly, while most of the discussions in the literature are performed at 300–800 K where the thermoelectric applications are most relevant.[14] Therefore, it is better to focus on providing useful information about how the added electrons would populate the conduction band by potassium doping on the surface rather than looking for a direct signature of the conduction band in our low-temperature ARPES results.

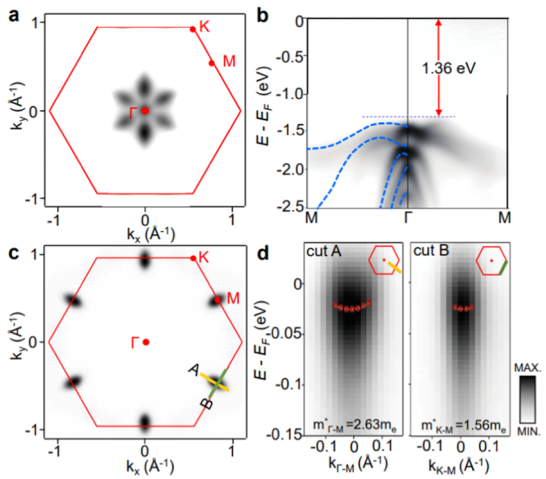

Figure 6. Electronic band structure of pristine and potassium (K)-doped $SnSe_2$ single crystals. (a) Constant energy contour of pristine $SnSe_2$ for a binding energy of −1.36 eV. (b) ARPES spectra of pristine $SnSe_2$ along the Γ-M direction with VBM at 1.36 eV below E_F. The blue dotted lines are the calculated band structures (density functional theory (DFT)) adapted from ref 14. Copyright © 2019 AIP Publishing. (c) Fermi surface of K-doped $SnSe_2$ with conduction bands at M points. (d) Electronic structures along the momentum directions, A and B, in (c). Red dots are the peaks of EDCs fitted by the Gaussian function, and orange curves indicate the fitted parabolic curves near the band bottom to extract the effective mass.

To achieve high ZT for a thermoelectric material, band engineering is proposed as an effective strategy, but the resulting enhancement is often subtle due to the competition among the factors constituting the ZT value. ZT is determined by electrical conductivity, Seebeck coefficient, and thermal conductivity, which depend on the charge carrier concentration (*n*) in a conflicting manner, suggesting that optimizing *n* is a significant strategy for enhancing the ZT. For $SnSe_2$, ZT maximizes when *n* is around 10^{20} cm^{-3}, which is higher than the *n* of pristine $SnSe_2$ ($\sim 10^{18}$ cm^{-3}).[14] Our ARPES data clearly shows that electron doping fills up the conduction bands rather than forming the in-gap states, resulting in the metallic band character (Figure 6c,d), which is in contrast to the semiconducting band character of pristine $SnSe_2$ (Figure 6a,b). This proposes that thermoelectric properties of tin diselenide can be improved by enhancing *n*, yielding the changes in the band character from semiconducting with $n \sim 10^{18}$ cm^{-3} to metallic with $n \sim 10^{20}$ cm^{-3}, induced by electron doping.

According to the calculations of the partial and total density of state (DOS) for $SnSe_2$,[30] the Sn 4*p* orbitals mainly contribute to the lowest conduction bands, in which the contribution of Se $4p_z$ is less than that of Se $4p_x$ and $4p_y$. This leads to the superiority of in-plane electrical conductivity compared to the out-of-plane direction. However, with increasing carrier concentration by heavy donor doping, the carriers will fill Se $4p_z$ partially when Se $4p_x$ and $4p_y$ are already filled, leading to a steady increase in out-of-plane electrical conductivity. Thus, theoretical calculations support our higher ZT_c of 0.15 along the *c*-axis, compared to ZT_{ab} of 0.1 in the *ab* plane, indicating better out-of-plane thermoelectric properties. We expect significant boost of thermoelectric performance in out-of-plane ZT_c, when $SnSe_2$ can be heavily electron-doped.

4. CONCLUSIONS

In summary, we synthesized a high-quality $SnSe_2$ single crystal using the temperature gradient method. The bulk material showed strong anisotropy in both electrical and thermal conductivities. An ultralow thermal conductivity κ_c= 0.43 W m^{-1} K^{-1} was obtained at 673 K, which creates a favorable condition to enhance thermoelectric performance. The out-of-plane thermoelectric figure-of-merit (ZT_c) value is 0.15 at 673 K, which is higher than the in-plane one because of the lower out-of-plane thermal conductivity of $SnSe_2$ single crystals. ARPES data predicts that the power factor can be significantly improved via electronic doping.

AUTHOR INFORMATION

Corresponding Authors

Anh-Tuan Duong − *Phenikaa Research and Technology Institute (PRATI) and Faculty of Materials Science and Engineering, Phenikaa University, Hanoi 12116, Vietnam*; Email: tuan.duonganh@phenikaa-uni.edu.vn

Sunglae Cho − *Department of Physics and Energy Harvest-Storage Research Center, University of Ulsan, Ulsan 44610, Republic of Korea*; orcid.org/0000-0001-9154-3550; Email: slcho@ulsan.ac.kr

https://dx.doi.org/10.1021/acsaem.0c01846
ACS Appl. Energy Mater. XXXX, XXX, XXX−XXX

Authors

Anh-Tuan Pham − *Department of Physics and Energy Harvest-Storage Research Center, University of Ulsan, Ulsan 44610, Republic of Korea*

Thi Hoa Vu − *Department of Physics and Energy Harvest-Storage Research Center, University of Ulsan, Ulsan 44610, Republic of Korea;* orcid.org/0000-0001-6507-7242

Chang Cheng − *School of Materials Science and Engineering, Beihang University, Beijing 100191, China*

Thi Ly Trinh − *Department of Physics and Energy Harvest-Storage Research Center, University of Ulsan, Ulsan 44610, Republic of Korea*

Ji-Eun Lee − *Center for Spintronics, Korea Institute of Science and Technology (KIST), Seoul 02792, Republic of Korea; Department of Physics, Pusan National University, Busan 46241, Republic of Korea*

Hyejin Ryu − *Center for Spintronics, Korea Institute of Science and Technology (KIST), Seoul 02792, Republic of Korea;* orcid.org/0000-0003-3600-9755

Choongyu Hwang − *Department of Physics, Pusan National University, Busan 46241, Republic of Korea;* orcid.org/0000-0003-2989-475X

Sung-Kwan Mo − *Advanced Light Source, Lawrence Berkeley National Laboratory, Berkeley, California 94720, United States;* orcid.org/0000-0003-0711-8514

Jungdae Kim − *Department of Physics and Energy Harvest-Storage Research Center, University of Ulsan, Ulsan 44610, Republic of Korea;* orcid.org/0000-0002-8567-1529

Li-dong Zhao − *School of Materials Science and Engineering, Beihang University, Beijing 100191, China;* orcid.org/0000-0003-1247-4345

Complete contact information is available at: https://pubs.acs.org/10.1021/acsaem.0c01846

Author Contributions

The manuscript was written through the contribution of all authors. All authors have given approval to the final version of the manuscript.

Funding

This research is funded by the National Research Foundation of Korea (NRF-2019R1F1A1058473, NRF-2019R1A6A1A11053838, and NRF-2020K1A4A7A02095438) and Vietnam's National Foundation for Science and Technology Development (NAFOSTED) under grant number 103.02-2019.354.

Notes

The authors declare no competing financial interest.

■ ACKNOWLEDGMENTS

H.R. and J.-E.L. acknowledge the KIST Institutional Program (2E29410) and the National Research Foundation (NRF) of Korea (MSIT; 2019K1A3A7A09033388 and NRF-2020R1A5A1104591). This research used resources of the Advanced Light Source, a U.S. DOE Office of Science User Facility under contract no. DE-AC02-05CH11231. C.H. also acknowledges support from the National Research Foundation of Korea (NRF) grant funded by the Korea Government (MIST; Nos. 2018R1A2B6004538 and 2020K1A3A7A09080369).

■ REFERENCES

(1) Tritt, T. M.; Subramanian, M. A. Thermoelectric Materials, Phenomena, and Applications: A Bird's Eye View. *MRS Bull.* **2006**, *31*, 188−198.

(2) Gaultois, M. W.; Sparks, T. D.; Borg, C. K. H.; Seshadri, R.; Bonificio, W. D.; Clarke, D. R. Data-Driven Review of Thermoelectric Materials: Performance and Resource Considerations BT - Chemistry of Materials. *Chem. Mater.* **2013**, *25*, 2911−2920.

(3) Zhao, L.-D.; Lo, S.-H.; Zhang, Y.; Sun, H.; Tan, G.; Uher, C.; Wolverton, C.; Dravid, V. P.; Kanatzidis, M. G. Ultralow Thermal Conductivity and High Thermoelectric Figure of Merit in SnSe Crystals. *Nature* **2014**, *508*, 373−377.

(4) Duong, A. T.; Nguyen, V. Q.; Duvjir, G.; Duong, V. T.; Kwon, S.; Song, J. Y.; Lee, J. K.; Lee, J. E.; Park, S.; Min, T.; Lee, J.; Kim, J.; Cho, S. Achieving ZT = 2.2 with Bi-Doped n-Type SnSe Single Crystals. *Nat. Commun.* **2016**, *7*, No. 13713.

(5) Chang, C.; Wu, M.; He, D.; Pei, Y.; Wu, C. F.; Wu, X.; Yu, H.; Zhu, F.; Wang, K.; Chen, Y.; Huang, L.; Li, J. F.; He, J.; Zhao, L. D. 3D Charge and 2D Phonon Transports Leading to High Out-of-Plane ZT in n-Type SnSe Crystals. *Science* **2018**, *360*, 778−783.

(6) Julien, C.; Eddrief, M.; Samaras, I.; Balkanski, M. Optical and Electrical Characterizations of SnSe, SnS2 and SnSe2 Single Crystals. *Mater. Sci. Eng. B* **1992**, *15*, 70−72.

(7) Domingo, G.; Itoga, R. S.; Kannewurf, C. R. Fundamental Optical Absorption in SnS2 and SnSe2. *Phys. Rev.* **1966**, *143*, 536−541.

(8) Chung, K.-M.; Wamwangi, D.; Woda, M.; Wuttig, M.; Bensch, W. Investigation of SnSe, SnSe2, and Sn2Se3 Alloys for Phase Change Memory Applications. *J. Appl. Phys.* **2008**, *103*, No. 083523.

(9) Li, M. O.; Esseni, D.; Nahas, J. J.; Jena, D.; Xing, H. G. Two-Dimensional Heterojunction Interlayer Tunneling Field Effect Transistors (Thin-TFETs). *IEEE J. Electron Devices Soc.* **2015**, *3*, 200−207.

(10) Roy, T.; Tosun, M.; Hettick, M.; Ahn, G. H.; Hu, C.; Javey, A. 2D-2D Tunneling Field-Effect Transistors Using WSe2/SnSe2 Heterostructures. *Appl. Phys. Lett.* **2016**, *108*, No. 083111.

(11) Rai, R. K.; Islam, S.; Roy, A.; Agrawal, G.; Singh, A. K.; Ghosh, A.; Ravishankar, N. Morphology Controlled Synthesis of Low Bandgap SnSe2 with High Photodetectivity. **2019**, *2* 870 877. DOI: 10.1039/c8nr08138g.

(12) Saha, S.; Banik, A.; Biswas, K. Few-Layer Nanosheets of n-Type SnSe 2. *Chem. - Eur. J.* **2016**, *22*, 15634−15638.

(13) Li, G.; Ding, G.; Gao, G. Thermoelectric Properties of SnSe2 Monolayer. *J. Phys.: Condens. Matter* **2017**, *29*, No. 015001.

(14) Ding, Y.; Xiao, B.; Tang, G.; Hong, J. Transport Properties and High Thermopower of SnSe2: A Full Ab-Initio Investigation. *J. Phys. Chem. C* **2017**, *121*, 225−236.

(15) Xu, P.; Fu, T.; Xin, J.; Liu, Y.; Ying, P.; Zhao, X.; Pan, H.; Zhu, T. Anisotropic Thermoelectric Properties of Layered Compound SnSe2. *Sci. Bull.* **2017**, *62*, 1663−1668.

(16) Li, F.; Zheng, Z.; Li, Y.; Wang, W.; Li, J. F.; Li, B.; Zhong, A.; Luo, J.; Fan, P. Ag-Doped SnSe2 as a Promising Mid-Temperature Thermoelectric Material. *J. Mater. Sci.* **2017**, *52*, 10506−10516.

(17) Wu, Y.; Li, W.; Faghaninia, A.; Chen, Z.; Li, J.; Zhang, X.; Gao, B.; Lin, S.; Zhou, B.; Jain, A.; Pei, Y. Promising Thermoelectric Performance in van Der Waals Layered SnSe 2. *Mater. Today Phys.* **2017**, *3*, 127−136.

(18) Choi, J.; Lee, H.; Kim, B.; Park, H.; Choi, S.; Hong, S. C.; Cho, S. Magnetic and Transport Properties of Mn-Doped Bi 2 Se 3 and Sb 2 Se 3. *J. Magn. Magn. Mater.* **2006**, *304*, 164−166.

(19) Wiedemeier, H.; Pultz, G.; Gaur, U.; Wunderlich, B. Heat Capacity Measurements of SnSe and SnSe2. *Thermochim. Acta* **1981**, *43*, 297−303.

(20) Kim, H. S.; Gibbs, Z. M.; Tang, Y.; Wang, H.; Snyder, G. J. Characterization of Lorenz Number swith Seebeck Coefficient Measurement. *APL Mater.* **2015**, *3*, No. 041506.

(21) Liu, M.; Zhang, J.; Xu, J.; Hu, B.; Sun, K.; Yang, Y.; Wang, J.; Du, B.; Zhang, H. The Crystallization, Thermodynamic and

Thermoelectric Properties of Vast off-Stoichiometric Sn−Se Crystals. *J. Mater. Chem. C* **2020**, *8*, 6422−6434.
(22) Shu, Y.; Su, X.; Xie, H.; Zheng, G.; Liu, W.; Yan, Y.; Luo, T.; Yang, X.; Yang, D.; Uher, C.; Tang, X. Modification of Bulk Heterojunction and Cl Doping for High-Performance Thermoelectric SnSe2/SnSe Nanocomposites. *ACS Appl. Mater. Interfaces* **2018**, *10*, 15793−15802.
(23) Liu, M.; Zhang, J.; Xu, J.; Hu, B.; Liu, B.; Sun, K.; Yang, Y.; Wang, J.; Du, B. Phase Structure, Phase Transition and Thermoelectric Properties of Pristine and Br Doped SnSe2. *J. Solid State Chem.* **2020**, *289*, No. 121468.
(24) Busch, G.; Fröhlich, C.; Hulliger, F.; Steigmeier, E. Struktur, Elektrische und Thermoelektrische Eigenschaften von SnSe2. *Helv. Phys. Acta* **1961**, *34*, 359−368.
(25) Wang, H.; Gao, Y.; Liu, G. Anisotropic Phonon Transport and Lattice Thermal Conductivities in Tin Dichalcogenides SnS2 and SnSe2. *RSC Adv.* **2017**, *7*, 8098−8105.
(26) Li, G.; Ding, G.; Gao, G. Thermoelectric Properties of $SnSe_2$ Monolayer. *J. Phys.: Condens. Matter* **2017**, *29*, No. 015001.
(27) Lochocki, E. B.; Vishwanath, S.; Liu, X.; Dobrowolska, M.; Furdyna, J.; Xing, H. G.; Shen, K. M. Electronic Structure of SnSe2 Films Grown by Molecular Beam Epitaxy. *Appl. Phys. Lett.* **2019**, *114*, No. 091602.
(28) Kim, S., Il; Hwang, S.; Kim, S. Y.; Lee, W.-J.; Jung, D. W.; Moon, K.-S.; Park, H. J.; Cho, Y.-J.; Cho, Y.-H.; Kim, J.-H.; Yun, D.-J.; Lee, K. H.; Han, I.; Lee, K.; Sohn, Y. Metallic Conduction Induced by Direct Anion Site Doping in Layered SnSe2. *Sci. Rep.* **2016**, *6*, No. 19733.
(29) Rasmussen, F. A.; Thygesen, K. S. Computational 2D Materials Database: Electronic Structure of Transition-Metal Dichalcogenides and Oxides. *J. Phys. Chem. C* **2015**, *119*, 13169−13183.
(30) Bletskan, D. I. Electronic Structure of 2H-SnSe2: Ab Initio Modeling and Comparison with Experiment. *Semicond. Phys., Quantum Electron. Optoelectron.* **2016**, *19*, 98−108.

https://dx.doi.org/10.1021/acsaem.0c01846
ACS Appl. Energy Mater. XXXX, XXX, XXX−XXX